



Prostaglandin E₂ promotes pathological retinal neovascularisation via EP₄R-EGFR-Gab1-AKT signaling pathway

Tianhua Xie^{a,b,c,1}, Zhonghong Zhang^{a,d,1}, Yuqing Cui^a, Yishun Shu^a, Yanqiu Liu^a, Jian Zou^b, Man Wang^a, Yangningzhi Wang^a, Qian Yang^{a,b}, Xubin Pan^e, Jiping Cai^a, Xiaodong Sun^c, Yong Yao^{a,*}, Xiaolu Wang^{a,b,**}

^a Department of Ophthalmology, The Affiliated Wuxi People's Hospital of Nanjing Medical University, 299 Qingyang Road, Wuxi, Jiangsu, 214023, PR China

^b Center of Clinical Research, The Affiliated Wuxi People's Hospital of Nanjing Medical University, 299 Qingyang Road, Wuxi, Jiangsu, 214023, PR China

^c Department of Ophthalmology, Shanghai General Hospital of Nanjing Medical University, Shanghai, 200080, PR China

^d Department of Ophthalmology, Zhongda Hospital Southeast University, 87 Dingjiaqiao, Nanjing, Jiangsu, 210009, PR China

^e Department of Ophthalmology, Affiliated Hospital of Jiangnan University, 200 Huihe Road, Wuxi, Jiangsu, 214062, PR China

ARTICLE INFO

Keywords:

PGE₂
EP₄R
EGF receptor
Retinal angiogenesis
Endothelial cell

ABSTRACT

Proliferative retinopathies, such as proliferative diabetic retinopathy (PDR) and retinopathy of prematurity (ROP) are major causes of visual impairment and blindness in industrialized countries. Prostaglandin E₂ (PGE₂) is implicated in cellular proliferation and migration via E-prostanoid receptor (EP₄R). The aim of this study was to investigate the role of PGE₂/EP₄R signaling in the promotion of retinal neovascularisation. In a streptozotocin (STZ)-induced diabetic model and an oxygen-induced retinopathy (OIR) model, rats received an intravitreal injection of PGE₂, cay10598 (an EP₄R agonist) or AH23848 (an EP₄R antagonist). Optical coherence tomography, retinal histology and biochemical markers were assessed. Treatment with PGE₂ or cay10598 accelerated pathological retinal angiogenesis in STZ and OIR-induced rat retina, which was ameliorated in rats pretreated with AH23848. Serum VEGF-A was upregulated in the PGE₂-treated diabetic rats vs non-treated diabetic rats and significantly downregulated in AH23848-treated diabetic rats. PGE₂ or cay10598 treatment also significantly accelerated endothelial tip-cell formation in new-born rat retina. In addition, AH23848 treatment attenuated PGE₂- or cay10598-induced proliferation and migration by repressing the EGF receptor (EGFR)/Growth factor receptor bound protein 2-associated binder protein 1 (Gab1)/Akt/NF-κB/VEGF-A signaling network in human retinal microvascular endothelial cells (hRMECs). PGE₂/EP₄R signaling network is thus a potential therapeutic target for pathological intraocular angiogenesis.

1. Introduction

Neovascularisation (NV) is essential for embryonic development. Rat retinal vessels grow postnatally from the central optic disk radially to the periphery in response to a VEGF-A gradient, as rats are born with avascular retinas. The primary superficial vascular network is established within 7 days, and the established vascular plexus then undergoes remodelling to complete the vascular network (Stahl et al., 2010; Yang et al., 2015). This embryo-fetal programme reactivates at the adult, for

instance, during tissue growth, wound healing or the menstrual cycle. However, uncontrolled or excessive vessel sprouting results in a lot of diseases (Chung and Ferrara, 2011). In eyes, proliferative vitreoretinal NV, including proliferative diabetic retinopathy (PDR), retinopathy of prematurity (ROP), and retinal vein occlusion, are the main causes of visual impairment and blindness in many countries (Reynolds, 2014; Fong et al., 2004; Laouri et al., 2011; Laatikainen et al., 2016). Rapidly growing vasculature is immature and lead to leakage an abundance of cellular contents including proangiogenic factors and proinflammatory

* Corresponding author. Department of Ophthalmology, The Affiliated Wuxi People's Hospital of Nanjing Medical University, 299 Qingyang Road, Wuxi, Jiangsu, 214023, PR China.

** Corresponding author. Center of Clinical Research, The Affiliated Wuxi People's Hospital of Nanjing Medical University, 299 Qingyang Road, Wuxi, Jiangsu, 214023, PR China.

E-mail addresses: yongyao@njmu.edu.cn (Y. Yao), xlwang@njmu.edu.cn (X. Wang).

¹ Tianhua Xie and Zhonghong Zhang contributed equally to this work.

<https://doi.org/10.1016/j.exer.2021.108507>

Received 28 September 2020; Received in revised form 25 January 2021; Accepted 12 February 2021

Available online 17 February 2021

0014-4835/© 2021 Elsevier Ltd. All rights reserved.

cytokines/chemokines (Sapieha et al., 2010). VEGF-A is a vasoactive factor mediated endothelial cell proliferation and tube formation, which has been implicated in angiogenesis and hyperpermeability processes. The employment of anti-VEGF-A agents is an emerging treatment for PDR or acute ROP; however, long-term effects of such drugs are still rare, and there is an urgent need to find novel interventional approaches (Hartnett, 2020).

Prostanoids, a large family of bioactive lipids derived from the activity of COX1 and COX2, is a crucial growth-factor inducer and a potent proangiogenic mediator (Capra et al., 2014). Thromboxane A₂ (TXA₂) is the prostanoid product of COX1 and works through the activation of TBXA2R. Besides TBXA2R is a rate-limiting enzyme coupled with COX1 in biosynthesis of TXA₂ (Wang et al., 2018; Lucotti et al., 2019). COX2 catalyzes the downstream production of prostanoids including PGE₂, which therefore binds to its G-protein-coupled plasma membrane receptors (E-prostanoid1, 2, 3 and 4 receptors [EP₁₋₄R]), inducing multiple signal transduction pathways activation that result in downstream responses (Hata and Breyer, 2004). The EP₁R mainly recruits the G α q protein and stimulates the level of intracellular calcium upregulation; the EP₂R and EP₄R bind to the G α s protein, induce adenylate cyclase activation and upregulate intracellular cAMP production. In contrast, the EP₃R couples with the G α i protein, inactivates adenylate cyclase and inhibits the formation of intracellular cAMP (Wu, 2005). It has been reported that PGE₂ significantly promotes cell growth and invasion via activation of the classical EP₄R/G α S/AC/cAMP/PKA signaling pathway in hepatocellular carcinoma cells (Xia et al., 2014). However, recent findings have reported that PGE₂ stimulates EP₄R and induces the formation of an EP₄R- β -arrestin1-Src complex, which may result in the EGF receptor (EGFR) transactivation (Buchanan et al., 2003, 2006; Ansari et al., 2008; Tan et al., 2017). Growth factor receptor bound protein 2 (Grb2) binds to EGFR, followed by the binding of Grb2-associated binder protein 1 (GAB1), and it continues to recruit p85 subunit of PI3K in order to prolong or amplify the activation of the Akt signaling pathway (Moran et al., 2004; Mouradian et al., 2014). These changes are concomitant with enhanced cell proliferation and differentiation in several cancer cell types and portal hypertensive gastropathy (Buchanan et al., 2003, 2006; Ansari et al., 2008; Tan et al., 2017).

Recent studies have shown that COX2 and PGE₂ are involved in the pathogenesis of retinal NV (Sennlaub et al., 2003; Schoenberger et al., 2012; Yanni et al., 2009). In rat models of oxygen-induced retinopathy (OIR), cytosolic phospholipase A2, COX and VEGF-A are coordinately upregulated. Nonsteroidal anti-inflammatory drugs that inhibit COX and PG synthesis reduce the NV response in rodent models of OIR (Nandgaonkar et al., 1999; Sennlaub et al., 2003; Wilkinson-Berka et al., 2003; Castro et al., 2004). Moreover, the EP₄R agonist promotes VEGF-A production and, subsequently, Muller cells and endothelial cell proliferation in vitro (Cheng et al., 1998; Yanni et al., 2009). In receptor combination patterns, PGE₂ exhibits various biological effects, and the specific E-prostanoid receptors of PGE₂ that regulate endothelial cell proliferation and retinal NV have not been well illustrated. These findings prompted us to determine whether the PGE₂/EP₄R cascade mediates RMEC proliferation in retinal NV and to investigate the underlying molecular mechanisms.

2. Materials and methods

2.1. Animals and treatments

All animal studies were maintained in accordance with the ARVO Statement for the Use of Animals in Ophthalmic and Vision Research and were approved by the Nanjing Medical University requirements for humane animal care. Rats were purchased from the laboratory animal centre of The Academy of Military Medical Sciences (Beijing, China) and housed under standard conditions (22.5 °C and 42.5% humidity, under a 12 h/12 h light-dark cycle, using heated wood chip litter as bedding material) in the SPF (specific pathogen free) animal centre of Wuxi

People's Hospital Affiliated to Nanjing Medical University, and permitted ad libitum consumption of water. Rats were ventilated on corresponding days after being anesthetized with a mixture of ketamine and xylazine. When adequacy of anesthesia was monitored by observation of slow breathing, loss of muscular tone, and no response to surgical manipulation, the retinas were harvested for corresponding analyzes.

For the PDR model, male Sprague Dawley rats (220–250 g) at eight-week-old were randomly divided into groups: control; STZ + DMSO; STZ + PGE₂; STZ + cay10598 and STZ + AH23848. Diabetic rats were induced with an i.p. injection of STZ (60 mg·kg⁻¹ in 10 mM citrate buffer at pH 4.6), as previously reported (Deliyanti et al., 2012; Wilkinson-Berka et al., 2009). The blood glucose levels of rats >16.7 mM, indicating that diabetes had been successfully established. The STZ-treated rats were anesthetized (ketamine/xylazine), and given an intravitreal injection at a volume of about 5 μ l of the designated mixture for each eye using the 33-gauge needle every four weeks. Rats were sacrificed and their retinas collected at 5 months after diabetes was successfully established.

The OIR model was generated as described previously (Shan et al., 2017; Feenstra et al., 2019). Briefly, rat pups and their nursing mothers were exposed to 80% oxygen for 21 h/day and 20% O₂ for 3 h/day between postnatal day (P)0 to P11, and subsequently returned to normal room air from P12 to P18. Directly after their return to room air, randomly selected rats were intravitreally injected under anesthesia with 5 mM PGE₂, cay10598 (a PGE₂/EP₄R agonist) or AH23848 (an EP₄R antagonist) mixed with saline solution (154 mM NaCl) 1:3, at a total volume of 2 μ l for each eye with a 33-gauge needle (Hamilton, Bonaduz, Switzerland) under a surgical microscope in anesthetized rats on P12 of the OIR model. A mixture of one volume of saline solution with three volumes of DMSO was prepared for the vehicle control. Control animals received the same treatment of vehicle control and were housed under normal room air. Eyes were dissected under deep anesthesia at P18 to assess the effect of OIR. The five experimental groups were as follows: control; untreated OIR; OIR + PGE₂; OIR + cay10598; OIR + AH23848 and OIR + DMSO.

For the physiological retinal angiogenesis assay, intravitreal injection of PGE₂, cay10598 or AH23848 was performed in rat pups at P3. Two days later, the retinas were collected and fixed in ice-cold 4% paraformaldehyde (wt·vol⁻¹) overnight. Samples were permeabilized in a permeabilising buffer (0.5% Triton X-100 in PBS) for 1 h and were blocked in a blocking buffer (10% donkey serum, 0.2% Tween-20) for 1 h. Samples were then stained with isolectin B4 (IB4) antibodies (Invitrogen, Carlsbad, CA, USA, 1:1000) in PBS for 1 h. After the washing steps, the samples were mounted using a fluorescence mounting medium (Beyotime Biotechnology, Shanghai, China). A confocal microscope (Leica, Heidelberg, Germany) was used to acquire the digital images.

2.2. Retinal imaging

Rats were anesthetized. Cyclomydril (Alcon, Fort Worth, TX, USA) was used to dilated their pupils. Spectral domain optical coherence tomography (OCT) images were taken using the image-guided OCT system (Micron IV; Phoenix Research Labs, Pleasanton, CA, USA) with the guidance of a bright-field live fundus image.

2.3. Histological and immunohistochemical analysis

Rats were anesthetized (ketamine/xylazine), and their eyes were dissected and fixed in 4% paraformaldehyde (wt·vol.) overnight. The retinas and scleras were dehydrated in a graded ethanol series and embedded in paraffin. Standard immunohistochemical analysis using SABC and DAB kits (BOSTER, Wuhan, China) was performed to localize COX1 and COX2 expression as previously described (Han et al., 2020). For hematoxylin and eosin (H&E) staining, 5- μ m-thick sections were

taken along the vertical meridian. Digital images of H&E staining were observed under an Olympus BX-51 light microscope (Olympus, Tokyo, Japan).

2.4. Immunofluorescence analysis

Standard immunofluorescence analysis was performed to indicate Endoglin (CD105) (1: 1000, Abcam, MA, USA) expression, followed by Goat anti-Mouse IgG (H + L) Cross-Adsorbed Secondary Antibody, Alexa Fluor 555 and IB4 (1: 500, Life Technologies, CA, USA) in rat retinas as previously described (Han et al., 2020). DNA binding activity of NF- κ B translocation from the cytoplasm to the nucleus was evaluated by immunofluorescence using anti-NF- κ B subunit p65 (1: 400, Cell Signaling Technology, MA, USA). Monoclonal anti-Ki-67 antibody (1: 1000, Abcam, MA, USA) was used to mark the cell cycle in human retinal microvascular endothelial cells (hRMECs).

2.5. ELISA

Blood samples were collected during necropsy after a 12-hr fast by retro-orbital puncture. PGE₂ and TXB₂ in the vitreous fluid of individuals with diabetic retinopathy vs healthy individuals was measured using commercial ELISA kits (PGE₂: R&D Systems, Minneapolis, MN, USA and TXB₂: Abcam, Cambridge, MA, USA). VEGF-A in the serum of diabetic rats was measured using commercial ELISA kits (Cusabio, Wuhan, China).

2.6. Evans Blue

The retinal vessels in rats were marked with Evans Blue, which was described previously by Shan and colleagues (Shan et al., 2017). Rats were administered Evans blue (100 mg kg⁻¹) via the femoral vein and kept on a warm pad for 60 min. The eyes were collected and fixed in 4% paraformaldehyde (wt·vol⁻¹) for 2 h. The retinal flat mounts were acquired and mounted on glass slides and examined under an Olympus BX-51 light microscope (Olympus, Tokyo, Japan).

2.7. Cell culture

Human RMECs were >90% positive for acetylated low-density lipoprotein and obtained from BeNa Culture Collection (Beina Chuanglian Biotechnology Institute, Beijing, China) and cultured in DMEM supplemented with 10% FBS (vol/vol) and 1% antimycotics and antibiotics (vol/vol). Mycoplasma contamination was not detected. Besides, cells grown in DMEM were incubated with PGE₂ (10 μ M; Cayman Chemical Company, Ann Arbor, MI, USA) for 24 h. In some experiments, a selective NF- κ B inhibitor Pyrrolidine Dithiocarbamate (PDTC, 5 μ M) obtained from MedChemExpress, USA, and AH23848 (an EP₄R antagonist, 10 μ M), cay10598 (an EP₄R agonist, 10 μ M), SQ22536 (an adenylate cyclase inhibitor, 50 μ M), H89 (a PKA inhibitor, 5 μ M), LY294002 (a PI3K inhibitor, 10 μ M), AG1478 (an EGFR inhibitor, 100 μ M) obtained from Cayman Chemical Company (Ann Arbor, MI, USA) were added to cells 30 min before stimulation with PGE₂.

2.8. Electrophoretic mobility shift assay (EMSA)

The analysis of NF- κ B binding activity in nuclear proteins was performed as described in our previous study (Wu et al., 2014). NF- κ B binding activity was examined using a Light Shift Chemiluminescent EMSA kit (Thermo Fisher Scientific, Waltham, MA, USA) according to manufacturer's instructions. Briefly, nuclear proteins (5 μ g) were isolated from hRMECs. Specific unlabeled NF- κ B competitors (50- and 100-fold molar excess) were used along with the binding reaction mixture for the competition assay. A biotin endlabeled DNA duplex of sequences containing the NF- κ B binding site (5'-AGT TGA GGC GAC TTT CCC AGG C-3', 3'-TCA ACT CCG CTG AAA GGG TCC G-5') was incubated

with nuclear proteins at room temperature for 20 min. The reaction mixture was loaded onto 6% non-denaturing polyacrylamide gels and subsequently transferred to a nylon membrane (Hybond N+, Amersham Corp., Arlington Heights, IL). The membranes were exposed to ultraviolet light to cross-link proteins for 1 min and incubated with conjugate/blocking buffer with stabilized streptavidin horseradish peroxidase conjugate. The signal on the membranes was detected with the enhanced chemiluminescence system (West Pico kit, Pierce, Loughborough, UK). The membranes were then exposed to X-ray film for 2–6 min and the relative intensities were analyzed with Image J software.

2.9. Viability and proliferation (WST-1) assay

The cell proliferation reagent WST-1 (Beyotime Biotechnology, Shanghai, China) was used to assess the viability in 96-well culture cell plates as described previously (Mynampati et al., 2017). Briefly, the treated cells (5 \times 10⁴) were stained with WST at 37 °C for 2 h and quantified by measuring the absorbance at 450 nm and normalized with the control absorbance at 690 nm.

2.10. Dual-luciferase reporter assay

HEK293T cells were co-transfected with indicated VEGF promoter and reporter plasmids. After incubation for 24 h, relative luciferase activities were measured by Dual-Luciferase® Reporter (DLR™) Assay System (Promega, E1910) as described previously (Zhang et al., 2020).

2.11. Cell migration assays

Cell migration assays were performed in 12-well hanging insert units (Millipore, Billerica, MA, USA). Before the experiment, 1 ml DMEM was added to the lower chamber of the transwell and incubated overnight. HRMECs (5 \times 10⁴) were seeded to the upper chamber and 1 ml complete DMEM was added to the lower chamber of the transwell with pharmacological agents at the indicated time. After incubation at 37 °C for 12 h, the cells were fixed with 4% paraformaldehyde (wt/vol.) and then stained with 0.1% crystal violet for 30 min at room temperature. After the washing steps, the cells were removed by a moist cotton swab from the upper surface of the membrane. The cells that migrated to the lower surface of the membrane were solubilized with 300 μ l of 10% acetic acid and observed under a fluorescence microscope (EVOS FL Auto Imaging System, Life Technologies).

2.12. Small interfering RNA (siRNA) transfection

Gab1 siRNA#1~#3 (three independent siRNA sequence) was employed to inhibit the Gab1 expression, which was obtained from Ribobio (Guangzhou, China). The target sense sequence is 5'-CCAA-GAAGCCTATTCGTAT-3'. After hRMECs reached 70% confluence, cells were put on opti-MEM and subsequently transfected with siGab1 or siNC (non-genomic sequence) at concentrations of 20 nM for 4 h using the Lipofectamine 2000 transfection commercial kit (Invitrogen, Shanghai, China). Then opti-MEM was replaced by DMEM supplemented with 10% FBS. Subsequent experiments were performed 36 or 48 h later.

2.13. Western blot and immunoprecipitation analysis

Protein in cell lysates was analyzed by electrophoresis on an SDS-PAGE gel and transferred to PVDF membranes (Millipore, Billerica, MA, USA). Antibodies against p65, phospho-Akt (Thr308), 1: 1000; phospho-Akt (Ser473), 1: 1000; Akt, 1: 1000; phospho-EGFR, 1: 1000; EGFR, 1: 1000; phospho-Gab1, 1: 1000; Gab1, 1: 1000 were obtained from Cell Signaling Technology (Danvers, MA, USA). Antibody to the COX1, COX2, TBXAS1 (thromboxane A2 synthase), TBXA2R (thromboxane A2 receptor) and EP₄ receptor (1: 1000) were obtained from

Abcam (Cambridge, MA, USA). The β -actin antibody (1: 5000, Sigma-Aldrich, St. Louis, MO, USA), Tubulin (1: 1000, Abcam, Cambridge, MA, USA) and the Lamin B antibody (1: 1000, Abcam, Cambridge, MA, USA) were used to confirm equal protein loading among samples. The signal on the membranes was detected with an enhanced chemiluminescence system (West Pico kit, Pierce, Loughborough, UK). Band density was analyzed using the Image J software (National Institutes of Health imaging software).

For examination of the association of EGFR with EP₄R, cell lysates were immunoprecipitated with 2 μ g of anti-EP₄R antibody overnight at 4 °C. 25 μ l of protein A/G agarose beads (GE Healthcare, Pittsburgh, PA, USA) was added and incubated at 4 °C for another 4 h. After washing steps, the immunoprecipitates were resuspended with 30 μ l loading buffer and analyzed by western blot with EGFR antibody. The similar analysis was performed to examine of the association of Gab1 with EGFR. The list of antibodies is described in [Supplementary Table 1](#).

2.14. RNA quantification

RNA was extracted and analyzed by way of quantitative RT-PCR as described previously (Wang et al., 2017). The data were analyzed by using the $2^{-\Delta\Delta Ct}$ method and normalized to endogenous control β -actin (for rats) or GAPDH mRNA (for human), and the amount of target gene mRNA expression in each sample was expressed relative to that of control. Primer sequences for real-time quantitative PCR were designed by Primer Express Software (Thermo Fisher Scientific, Waltham, MA, USA; [Supplementary Table 2](#)).

2.15. Statistical analysis

The results are expressed as mean \pm SEM. ANOVA was used for multiple group comparisons, followed by Tukey's post hoc test. Tukey's post hoc test was run only if the F value achieved $P < 0.05$ and there was no significant variance in homogeneity. The data were analyzed using the GraphPad Prism-5 statistic software (Prism v5.0; GraphPad Software, La Jolla, CA, USA). A P value < 0.05 was considered statistically significant.

3. Results

3.1. PGE₂/EP₄R signaling influences retinal NV in diabetic rat retina

We evaluated the effect of prostanoids-associated signaling on pathological angiogenesis in STZ-induced diabetic rats. Interestingly, PGE₂ was upregulated in the vitreous fluid of the PDR participants compared with the healthy controls. However, the concentrations of TXB₂, a nonenzymatically produced stable metabolite of TXA₂, showed no significantly change in the vitreous fluid of individuals with diabetic retinopathy vs healthy individuals (Fig. 1A). Moreover, COX2 were dramatically increased in the retinal vascular of STZ-treated rats, while there was no significant difference of COX1 expression between groups (Fig. 1B and C). High-glucose stress resulted in a significant increase in COX2 and EP₄R expression compared with the control medium, and there is no significant difference in COX1, TBXAS1 and TBXA2R expression in the HG-treated cells (Fig. 1D–H). Taken together, this data suggests that COX2/PGE₂ signaling pathway is involved in retinal microvascular abnormality under diabetic conditions.

We further used intravitreal injection of PGE₂, cay10598 and AH23848 in STZ-induced diabetic rats every four weeks. Five months after diabetes was successfully established, the number of hyperreflective dots, the outpouching of internal limiting membrane (ILM) and the breach of ILM in superficial portion of inner retina in OCT images were significantly increased in 5-month diabetic rats compared with the control rats, and further increased in the PGE₂- and Cay10598-treated diabetic rats. In contrast, the AH23848 pre-treated group showed significantly improved morphology of the retinal layers under

diabetic conditions (Fig. 2A). A histological examination also showed that retinal vessels were potently exacerbated in the PGE₂- or cay10598-treated rats compared to the untreated diabetic rats. Moreover, rats pretreated with AH23848 demonstrated improved histological retinal changes under diabetic conditions (Fig. 2B and C).

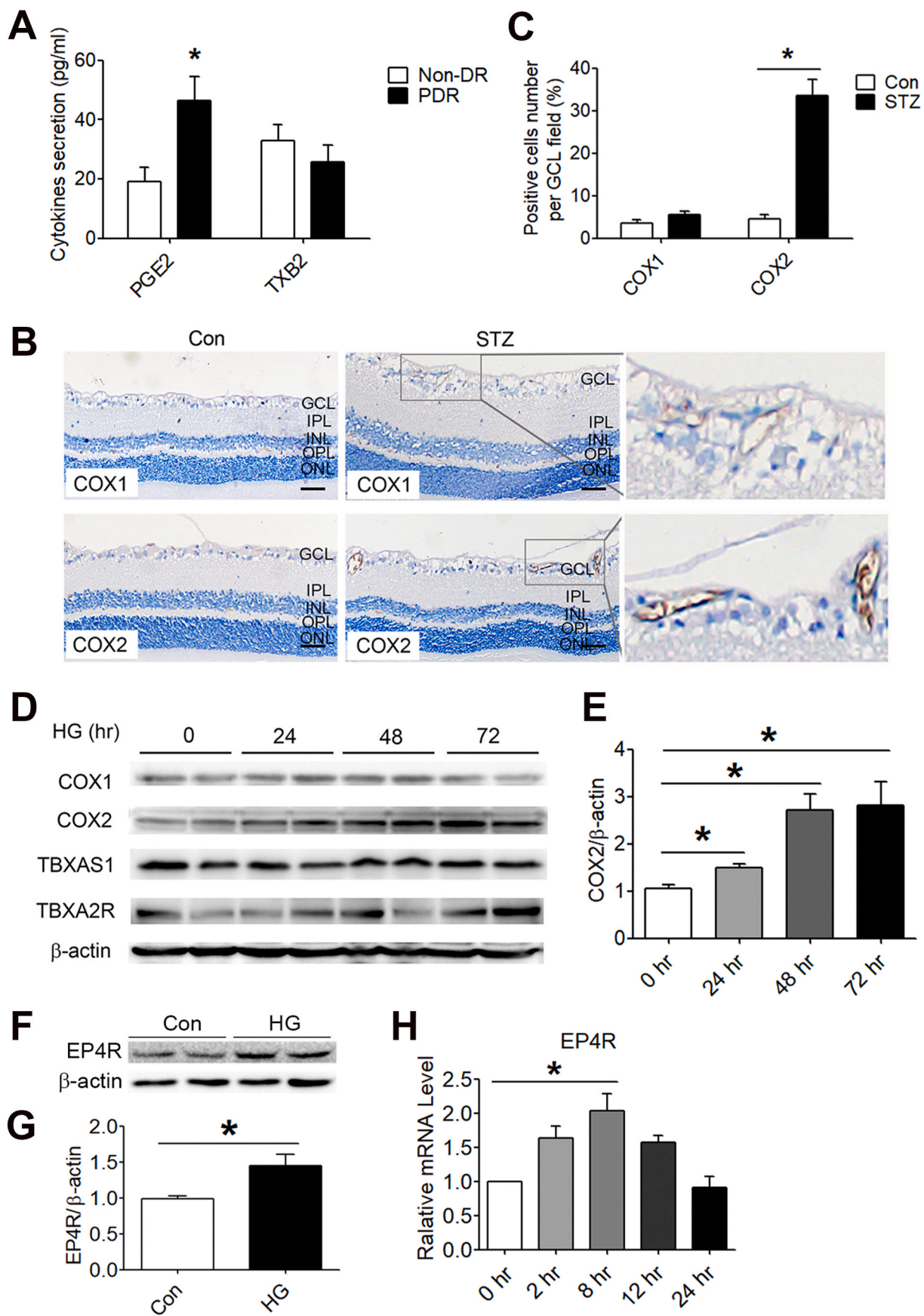
There is little or no expression of CD105 in quiescent endothelial cells, however, CD105 highly express in proliferating endothelial cells involved in active angiogenesis (Barnett et al., 2014; Dallas et al., 2008). It has been reported that retinal CD105 immunolocalization overlaps with nascent neovascular structures in OIR rats (Barnett et al., 2014). Thus, within the retina, CD105 could be a suitable target for imaging NV in retinal vascular diseases. Five months after successfully established diabetes, the PGE₂- or cay10598-treated groups displayed significantly increased amounts of diabetes-induced retinal NV as assessed by staining for CD105 and IB4. Interestingly, the rats treated with AH23848 exhibited decreased levels of retinal NV (Fig. 2D and E). Meanwhile, PGE₂-treated diabetic rats displayed significantly increased levels of VEGF-A, which was alleviated in rats that were pre-treated with AH23848 (Fig. 2F).

3.2. PGE₂/EP₄R signaling mediates postnatal retinal angiogenesis and VEGF-A expression in OIR rats

We employed the rat model of OIR, which is often applied to examine therapeutic substances or other treatments in ischemic retinal angiogenesis (Han et al., 2019, 2020). The fundus images showed that PGE₂- or cay10598-treated OIR rats displayed an increased formation of pathological vessels, as compared with the untreated OIR rats (Fig. 3A and B). OCT showed that both the number of hyperreflective dots (arrow) in the superficial portion of retinas and the number of hyporeflective spaces (triangle) in the inner retinal layers dramatically increased in the PGE₂- or cay10598-treated OIR pups. In contrast, the AH23848-pretreated group exhibited significantly improved morphology of the retinal layers under OIR conditions (Fig. 3A–C). H&E staining consistently indicated increased formation of pathological vessels in the retinas of PGE₂- or cay10598-treated rats and fewer pathological neovascular tufts in the retinas of the AH23848-treated rats (Fig. 3D and E).

Hyperoxia results in central vascular obliteration or degradation, and the subsequent relative hypoxia of room air leads to retinal NV in the OIR model (Han et al., 2019, 2020). We therefore evaluated the potential role of PGE₂/EP₄R signaling in OIR-induced retinal NV in the Evans blue-labelled retinal vessels of rats. The area of retinal NV tufts in the PGE₂- or cay10598-induced OIR rats was much greater than that of untreated OIR rats, whereas it is attenuated in AH23848-treated OIR rats. Further quantification showed that a 2.42-fold ($N = 6$, $P < 0.05$) and 2.63-fold ($N = 6$, $P < 0.05$) increase in the retinal NV tufts was observed in the PGE₂- and cay10598-treated OIR rats, respectively. A 0.8-fold ($N = 6$, $P < 0.05$) decrease in the retinal NV tufts was observed in the AH23848-treated OIR rats compared to the untreated OIR rats (Fig. 4A and B). This was consistent with the mRNA level of the vasoactive factor *Vegfa*, implicated in proliferative retinopathies (Fig. 4C). Taken together, these data suggest that PGE₂/EP₄R signaling can accelerate the retinal NV.

To further evaluate the effect of PGE₂/EP₄R signaling on blood vessels during sprouting angiogenesis, rats at were injected with PGE₂, cay10598, AH23848 or vehicle control medium in the vitreous humor at P3. Two days later, the retinas were collected for analysis. Whole-mount immunostaining of IB4 showed an increase in the vascularized area in PGE₂- or cay10598-treated retinas compared to the vehicle control treatment (Fig. 4D and E). Remarkably, the density of sprouting tips at the vascular front were also significantly increased in the PGE₂- or cay10598-treated groups (Fig. 4D and E), indicating that PGE₂/EP₄R signaling promoted tip-cell formation. However, rats pretreated with AH23848 did not exhibit physiologically impaired postnatal retinal angiogenesis. Hence, PGE₂/EP₄R signaling specifically promoted the



(caption on next page)

Fig. 1. COX2/PGE₂ signaling is engaged in abnormal changes in the retinal microvasculature experiencing high-glucose stress. (A) PGE₂ and TXB₂ was detected in the vitreous of healthy controls and proliferative diabetic retinopathy participants by ELISA; N = 6. (B) Immunohistochemistry for COX1 or COX2 (brown) and a hematoxylin nuclear counterstain (blue) was performed on retinal tissues obtained after 5 months after diabetes was successfully established; scale bar, 25 μm. (C) The quantification results are expressed as the ratio of positive cells numbers to total nuclear numbers in the GCL sections of retina; N = 6. (D–G) The level of COX1, COX2, TBXAS1, TBXA2R and EP₄R was determined by western blot. β-actin antibody was used to confirm equal protein loading among samples. Representative blots are shown, with quantification; N = 5. (H) Gene expression of EP₄R in retina of each group was detected by real-time PCR. The results are presented as means ± SEM; N = 5. The results are presented as means ± SEM; *P < 0.05 for each pair of groups indicated. Con, vehicle control-treated nondiabetic rats; GCL, ganglion cell layer; IPL, inner plexiform layer; INL, inner nuclear layer; OPL, outer plexiform layer; ONL, outer nuclear layer. (For interpretation of the references to colour in this figure legend, the reader is referred to the Web version of this article.)

formation of new vascular sprouts during retinal angiogenesis. Next, we sought to determine the functional significance of PGE₂/EP₄R signaling in mediating the expression of VEGF-A in hRMECs. Fig. 4F and G shows that PGE₂ and cay10598 significantly increased the expression of VEGF-A. In contrast, AH23848 treatment prevented PGE₂-induced VEGF-A up-regulation (Fig. 4F and G).

3.3. PGE₂/EP₄R signaling promotes hRMECs proliferation and migration via Akt activation

We examined the role of PGE₂/EP₄R signaling in hRMECs proliferation and migration using WST-1 assays and transwell migration assays as well as by observing the expression of cell cycle marker Ki67. The proliferation and migration were dramatically increased in PGE₂-or cay10598-treated hRMECs and decreased in AH23848-pretreated hRMECs, whereas SQ22536 (an adenylate cyclase inhibitor) or H89 (a PKA inhibitor) pretreatment, inhibiting the classical EP₄R/GαS/AC/cAMP/PKA signaling pathway could not attenuate PGE₂-or cay10598-induced proliferation and migration of hRMECs (Supplemental Figs. 1A–E). Our results demonstrated that PGE₂/EP₄R-induced proliferation and migration of hRMECs were independent of AC/cAMP/PKA signaling pathways. Moreover, we examined the abnormal activation of Akt, which is indeed critical for proliferation and migration in several cells. PGE₂ treatment potently induced phosphorylation of Akt at Thr308 and Ser473, which was reversed by pretreatment with AH23848 (Fig. 5A–D). Moreover, hRMECs pretreated with LY294002, a PI3K inhibitor, effectively abolished the proliferation and migration induced by PGE₂ and cay10598 exposure (Fig. 5E–I).

3.4. PGE₂ recruits EGFR to the EP₄R and enhances cellular proliferation via Akt activation

As noted above, PGE₂-activating EP₄R could cause the trans-activation of EGFR. Here, we observed an augmented formation of the EGFR-EP₄R complex in PGE₂-or cay10598-treated hRMECs (Fig. 6A and B). PGE₂ and cay10598 also induced a significant increase of phosphorylated EGFR (Fig. 6C and D). PGE₂ induced phosphorylation of Akt at Thr308, and Ser473 was also diminished in the cells pretreated with AG1478 (Fig. 6E–G). In addition, pretreatment of the hRMECs with AG1478, an EGFR inhibitor, dramatically inhibited PGE₂-and cay10598-induced the increase of VEGF-A expression (Fig. 6H and I). This was consistent with the proliferation and migration activity of hRMECs (Supplemental Figs. 2A–E).

3.5. EGFR recruits Gab1 and results in the upregulation of activated Akt

In addition, we observed an augmented formation of the Gab1-EGFR complex and an increased phosphorylation of Gab1 in PGE₂-or cay10598-treated hRMECs (Fig. 7A and B). hRMECs were transfected with siRNA-targeting Gab1 (siGab1) or a nontargeting siRNA control (siNC) for 48 h. The siRNA-expression vectors efficiently reduced the level of Gab1 in hRMECs (Supplemental Figs. 3A–C). Accordingly, the PGE₂-or cay10598-induced upregulation of Akt phosphorylation was reduced in siRNA-transfected cells (Fig. 7C and D). The distance in wound healing between the scorings in PGE₂-or cay10598-treated groups was shorter than in the control group. Moreover, in 24 h,

siGab1 pretreatment reduced the PGE₂-or cay10598-induced gaps between the scorings compared to the siNC-pretreated group (Fig. 7E and F).

3.6. PGE₂/EP₄R signaling increases NF-κB binding activity in hRMECs

Next, a pharmacological approach was used to determine whether PGE₂ regulated the expression of VEGF. Exogenous PGE₂ significantly increased the VEGF-A promoter activity, while treatment of AH23848, or LY294002, or AG1478 downregulated VEGF-A promoter activity (Fig. 8A). It has been reported that DNA binding activity of NF-κB was involved in PGE₂-induced VEGF-A production (Wu et al., 2013). In our study, treatment of the hRMECs with PGE₂ could increase the NF-κB translocation from the cytoplasm to the nucleus (Supplemental Figs. 4A and B). Meanwhile, AH23848 treatment dramatically prevented PGE₂ or cay10598 induced the p65 expression in the nucleus and DNA binding activity (Fig. 8B–F). Besides, a selective NF-κB inhibitor PDTC significantly inhibited PGE₂ and cay10598-induced VEGF-A expression in hRMECs (Fig. 8G and H).

4. Discussion

In the present study, we demonstrated the important role of PGE₂/EP₄R signaling pathway in hRMECs proliferation and retinal NV. We found that pathological retinal angiogenesis was ameliorated by inhibition of the PGE₂/EP₄R and EGFR/Gab1/Akt signaling network. This was associated with a decreased VEGF-A level. In Graphical Abstract, we demonstrated that the underlying mechanism of the effects of PGE₂/EP₄R signaling in pathological retinal NV.

STZ-induced diabetic model is one of the most commonly used models for many aspects of research in diabetes mellitus and displays phenotypical and histopathological features in consistent with PDR (Olivares et al., 2017). In the STZ-induced diabetic rats, vascular leakage, pericyte loss, increased acellular vessels, blood-retinal barrier breakdown and reduced visual function were found in early stages of DR at 2–3 months (Tzeng et al., 2015). Pre-proliferative stage of diabetic retinopathy was detected in the diabetic rats as early as 5–6 months, and exhibited endothelial cell proliferation, capillary dilation, and varicose loop formation (Olivares et al., 2017; Naderi et al., 2019). This pre-proliferative stage of diabetic retinopathy, or end-stage non-proliferative diabetic retinopathy in STZ-induced diabetic rats is corresponding to the intraretinal microvascular abnormality (IRMA) seen in human DR.

Recently, spectral domain OCT, a noninvasive imaging modality, has opened access to a broader sample of subjects, even diabetic retinopathy, infants and ROP subjects (Zepeda et al., 2018; Stoica et al., 2018; Bowl et al., 2016; Cernichiaro-Espinosa et al., 2016). In spectral-domain SD-OCT, the characteristics of IRMA in diabetic retinopathy were assessed for the presence of the following vitreous-retinal features: ① hyperreflective dots in superficial portion of inner retina without evidence of the ILM breach; ② the outpouching of ILM without disruption in the ILM layer; ③ the breach of ILM without the breach of posterior hyaloid or further growth into the core vitreous. In our study, the number of hyperreflective dots, the outpouching of ILM and the breach of ILM in superficial portion of inner retina in OCT images were significantly increased in 5-month diabetic rats compared with the

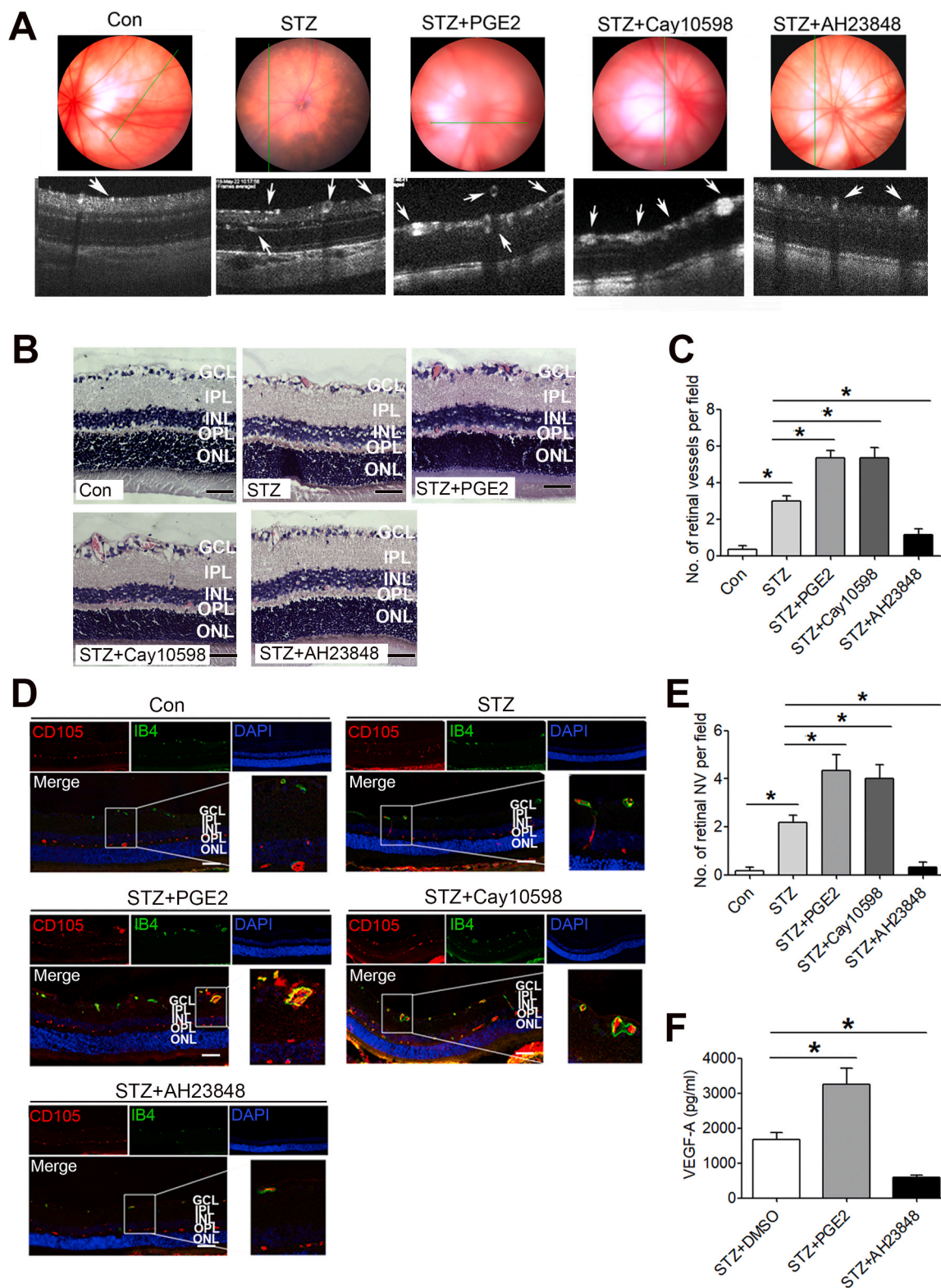


Fig. 2. PGE₂/EP₄R signaling regulates pathological angiogenesis in the retinas of STZ-induced diabetic rats. (A) Note the morphological changes in the color fundus images and the OCT images. (B) H&E staining in paraffin sections of rat retinas 5 months after establishment of the diabetes model; scale bar, 50 μm. (C) Quantification of vessel numbers in the retinal sections; N = 6. (D) Representative images of the immunofluorescence staining of CD105 (red) in the retinal sections of each group of rats. Retinal vessels were counterstained with (IB4, green); scale bar, 25 μm. (E) Quantification of vessels of angiogenesis in the retinal sections; N = 6. (F) Rat VEGF-A levels were detected in the serum of each group; N = 6. The results are presented as means ± SEM; *P < 0.05 for each pair of groups indicated. Con, vehicle control-treated nondiabetic rats; GCL, ganglion cell layer; IPL, inner plexiform layer; INL, inner nuclear layer; OPL, outer plexiform layer; ONL, outer nuclear layer. (For interpretation of the references to colour in this figure legend, the reader is referred to the Web version of this article.)

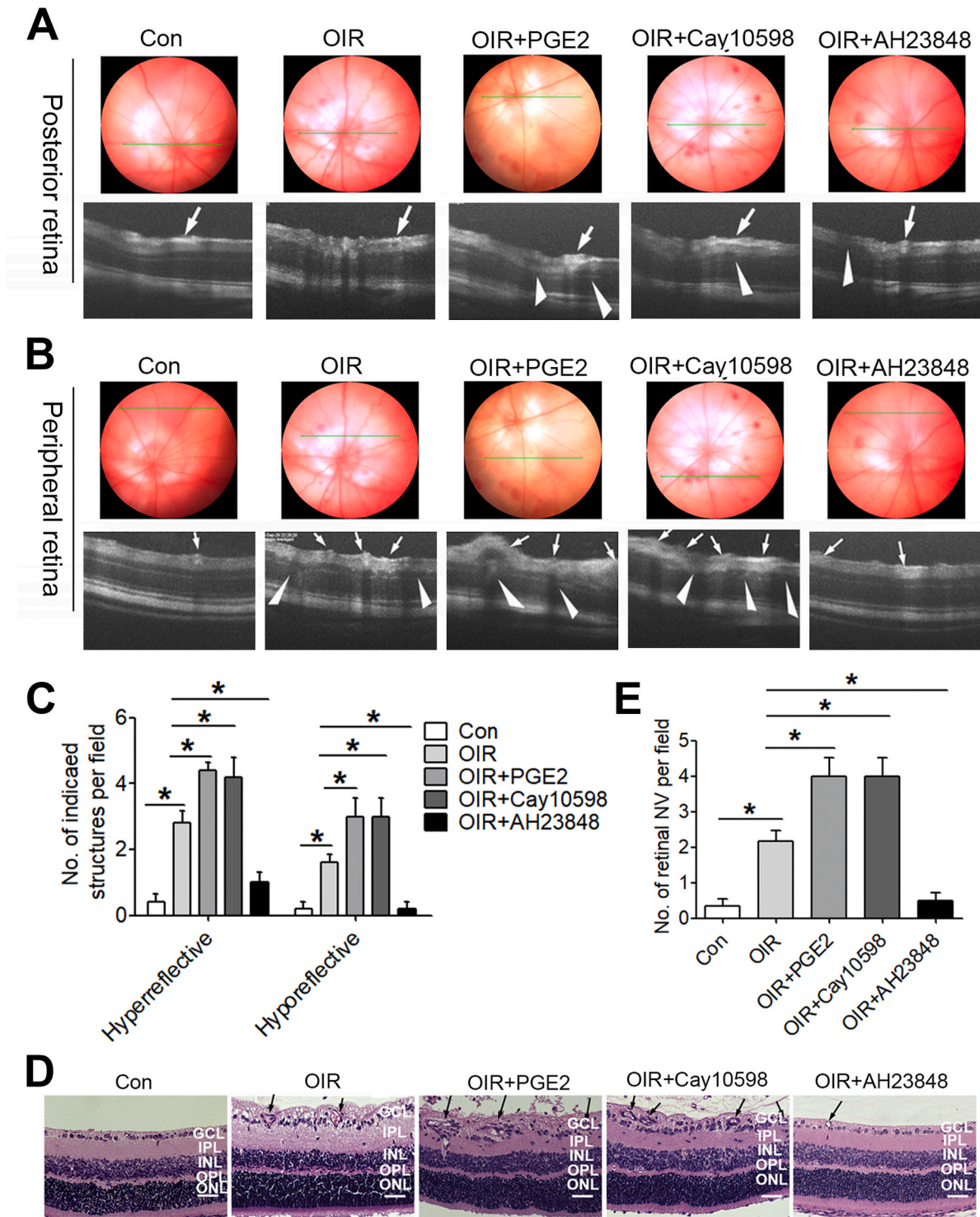


Fig. 3. PGE₂/EP₄R signaling mediates retinal angiogenesis in the eyes of OIR rats. (A-C) Note the morphological changes in the color fundus images and the OCT images. Retinal images of the posterior retina and peripheral retina were taken at P18 in the OIR rat model (A, B). The number of hyperreflective structures (arrows) and hyporeflective space (triangles) in the OCT images was determined (C); N = 6. (D, E) H&E staining in paraffin sections of rat retina at P18. Histological features of retinal NV (D); scale bar, 25 μm. Neovascularisation was assessed quantitatively by counting the endothelial cell nuclei anterior to the inner limiting membrane (E); N = 6. The results are presented as means ± SEM; *P < 0.05 for each pair of groups indicated. GCL, ganglion cell layer; IPL, inner plexiform layer; INL, inner nuclear layer; OPL, outer plexiform layer; ONL, outer nuclear layer. (For interpretation of the references to colour in this figure legend, the reader is referred to the Web version of this article.)

control rats, which are consistent with the characteristics of IRMA. Both PGE₂ and cay10598 aggravated the deleterious effects in STZ-induced diabetic rats. Likewise, we observed that PGE₂ and cay10598 treatment accelerated the occurrence of retinal NV and increased the central

proangiogenic factor VEGF-A. These effects were suppressed by AH23848 pretreatment.

Moreover, ROP shares many hallmarks with PDR, and both are regarded mainly as angiogenesis models (Chen et al., 2018). As an

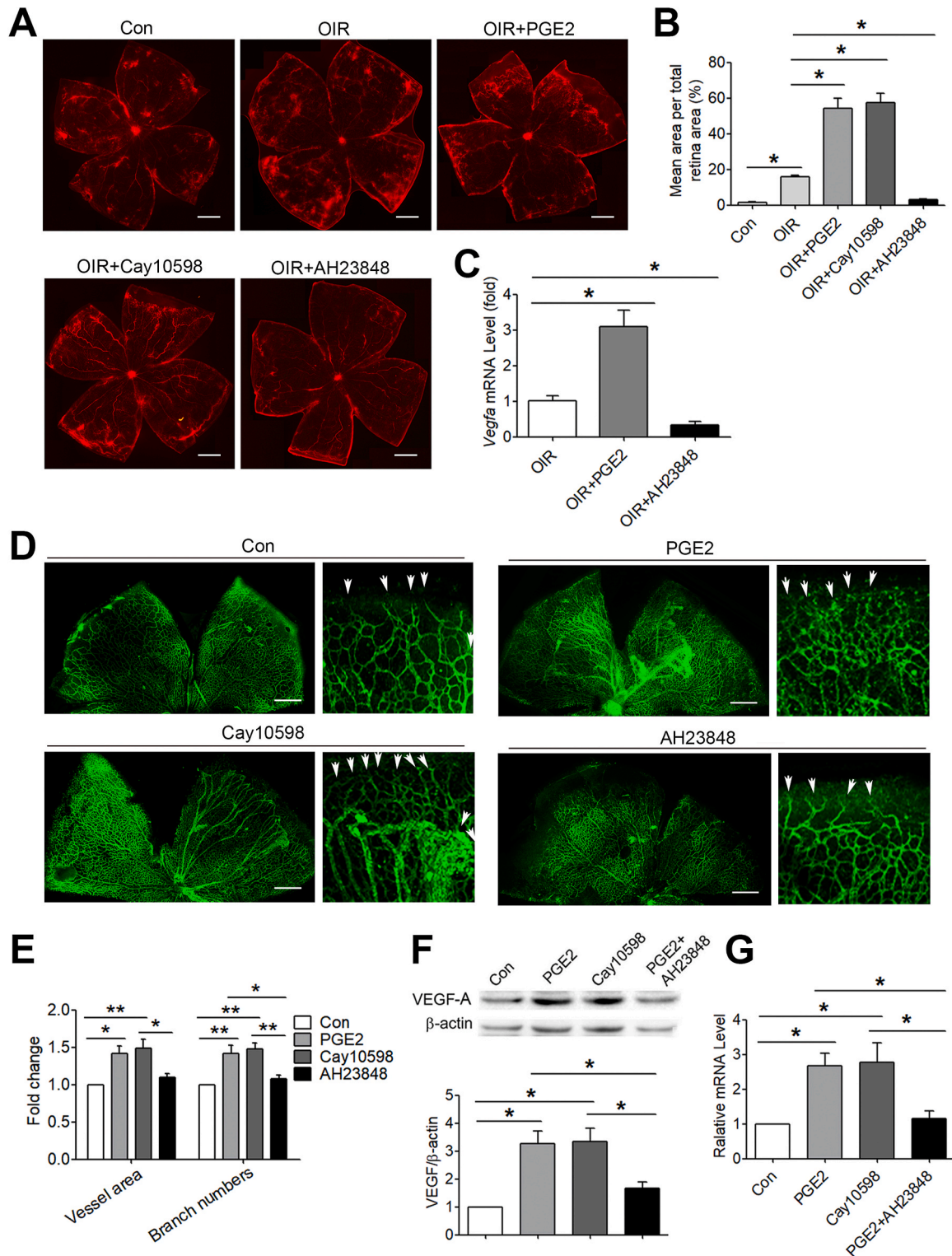


Fig. 4. PGE₂/EP₄R signaling mediates retinal NV and VEGF-A expression.

(A, B) Rats were infused with Evans Blue dye for 2 h

The fluorescence signal of NV (preretinal tufts) in the flat-mounted retina were detected using an Olympus BX-51 light microscope at × 4 objective (A); N = 6, scale bar, 100 μm. The quantification results are expressed as the ratio of NV area to total retinal area (B); N = 6. (C) Gene expression of *Vegfa* in retina of each group was detected by real-time PCR; N = 6. (D, E) Rat pups at P3 received PGE₂, cay10598, AH23848 or vehicle control medium. The retinal vasculature was examined at P5 by whole-mount IB4 (green) immunofluorescent staining. Representative images show the total retinal vasculature, retinal sprouting tips at the vascular front, and the enlarged intercapillary space (D); scale bar, 100 μm. Retinal vessel outgrowth measured as the total area from the central optic disk to the vascular front normalized to vehicle control treatment (E, left); N = 6. Number of sprouting tips per retina was determined (E, right); N = 6. (F) The level of VEGF-A was determined by western blot. β-actin antibody was used to confirm equal protein loading among samples; N = 5. (G) Gene expression of VEGF-A in hRMECs of each group was detected by real-time PCR; N = 5. The results are presented as means ± SEM; *P < 0.05 for each pair of groups indicated. Con, vehicle control-treated rats. (For interpretation of the references to colour in this figure legend, the reader is referred to the Web version of this article.)

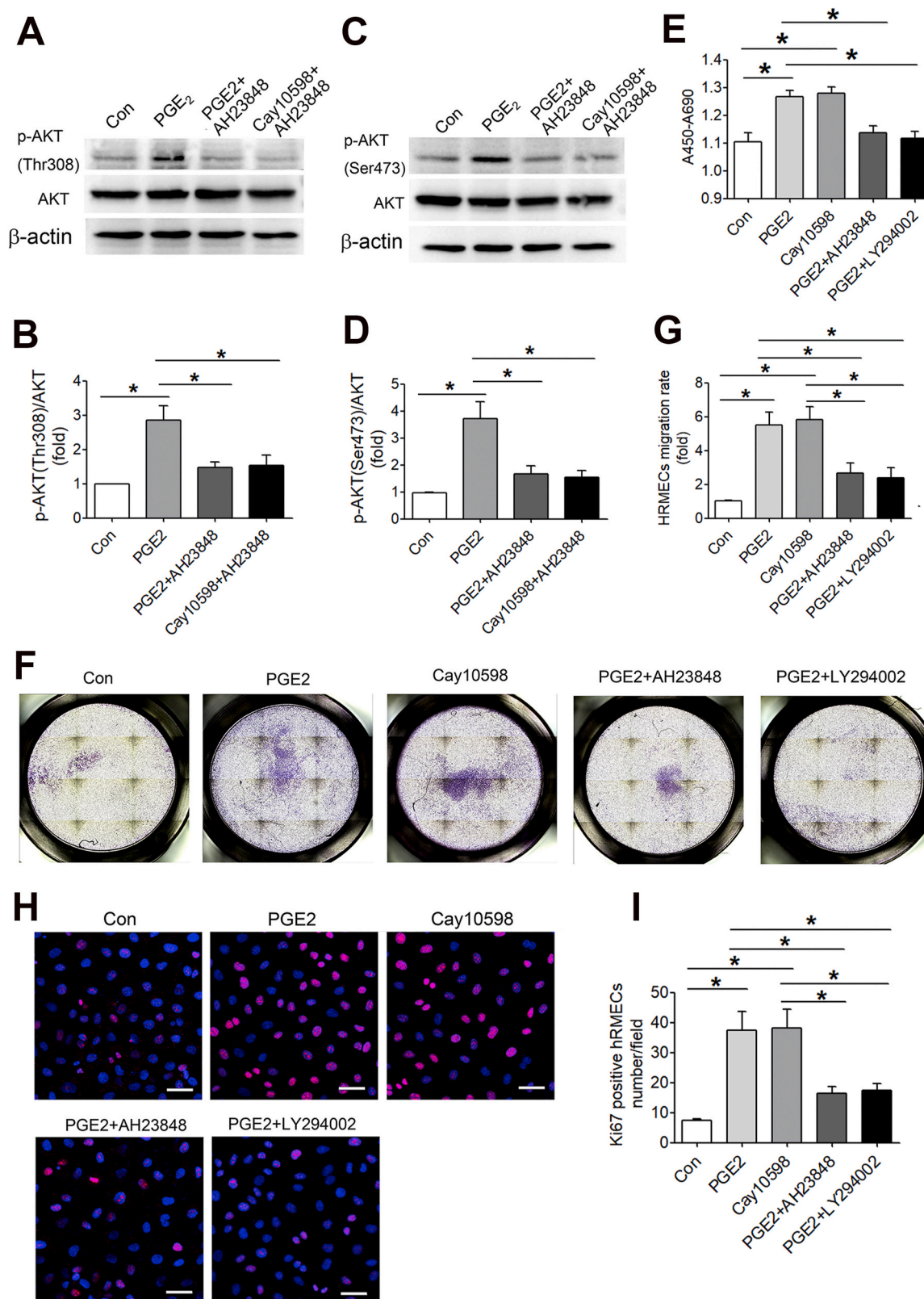


Fig. 5. The AKT activation was involved in PGE₂/EP₄R-signaling-mediated cellular proliferation and migration of hRMECs. (A-D) The levels of p-Akt (Thr308), p-Akt (Ser473) and Akt were determined by western blot. β-actin antibody was used to confirm equal protein loading among samples. Representative blots are shown, with quantification; N = 5. (E) Cell viability was assessed using the cell proliferation reagent WST; N = 5. (F, G) Migration of hRMECs in transwell assays was determined; N = 5. (H, I) A representative image was shown for Ki67 staining along with the quantification of Ki67 positive cells; scale bar, 25 μm; N = 5. The results are presented as means ± SEM; *P < 0.05 for each pair of groups indicated.

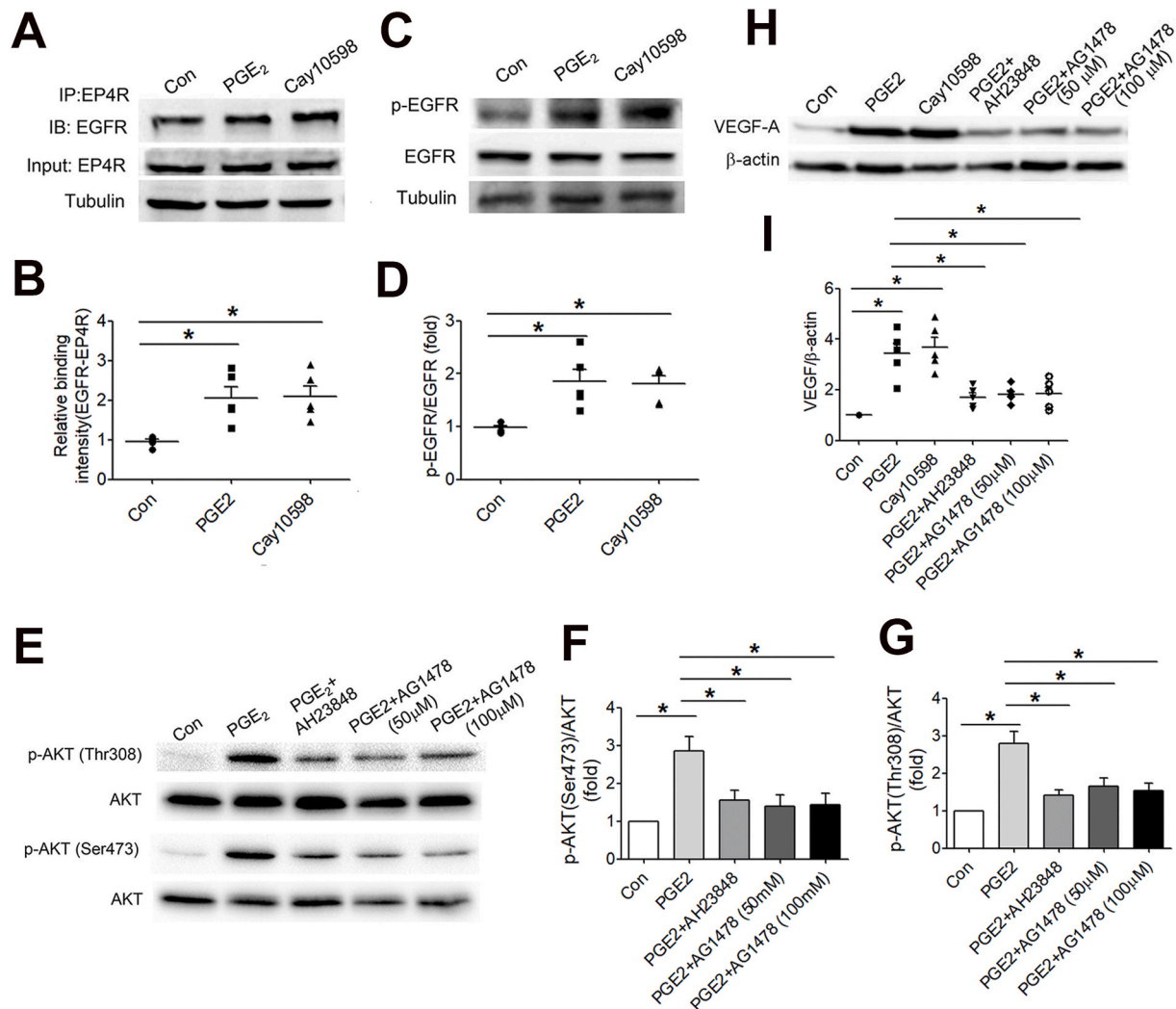


Fig. 6. PGE₂/EP₄R signaling promotes the proliferation and migration of hRMECs via transactivation of EGFR. (A, B) Immunoprecipitation was performed with anti-EP₄R antibody followed by immunoblotting with EGFR antibody. Representative blots are shown, with quantification; N = 5. (C, D) The levels of p-EGFR and EGFR were determined by western blot. Tubulin antibody was used to confirm equal protein loading among samples. Representative blots are shown, with quantification; N = 5. (E-G) The levels of p-Akt (Thr308), p-Akt (Ser473) and Akt were determined by western blot. Representative blots are shown, with quantification; N = 5. (H, I) The level of VEGF-A was determined by western blot; N = 5. The results are presented as means ± SEM; *P < 0.05 for each pair of groups indicated.

ocular disorder, ROP is characterized by an initial factor of relative ischemia, followed by abnormal NV that may culminate in the rapid outgrowth of pathological blood vessels from the retina to the vitreous humor and lens may lead to retinal hemorrhage, detachment and blindness (Wang et al., 2018). Both phases of ROP are reproduced by the rat OIR model, which can be used to test therapeutic substances or other treatments (Rivera et al., 2015). We treated rats with PGE₂, cay10598, AH23848 and DMSO by intravitreal injection, suggesting that their retinal effects are independent of any systemic activity. We observed that both PGE₂ and cay10598 could aggravate the deleterious effects of OIR-induced retinal angiogenesis, whereas the effects were ameliorated in the animal group that received the EP₄R antagonist AH23848.

The typical appearance of ROP as graded on spectral domain OCT is preretinal tissue and cystoid macular edema. The preretinal tissue on spectral domain OCT appears as a discrete hyperreflective laterally elongated structure with shadowing in the retinas of ROP subjects. The prevalence of cystoid macular edema in preterm infants screened for ROP is approximately 50%. These foveal cystoid structures appear as hyporeflective spaces in the inner nuclear layer (INL) in preterm infants. However, few studies have applied OCT to ROP rat pups (Erol et al., 2014; Lee et al., 2011; Rothman et al., 2015). In our study, consistent

with the histological examination, the OCT images revealed an increased number of discrete hyperreflective structures of preretinal tissues in the inner retina and hyporeflective spaces in the INL of foveal cystoid structures of PGE₂- or cay10598-treated OIR rats in the pups at P18.

In the OIR model, the NV (preretinal tufts) peaks at P18 (Han et al., 2019, 2020). We showed that retinas of OIR rats developed obliteration of the developing excessive pathological NV driven by retinal hypoxia at P18. Both PGE₂ and cay10598 aggravated the deleterious effects in OIR rats, whereas the effects were ameliorated in the animal group that received the EP₄R inhibitor AH23848.

Exaggerated sprouting angiogenesis is responsible for the rapid sprouting angiogenesis toward the vitreous body, which often results in vision loss (Sapieha et al., 2010; Yang et al., 2015). The shape, orientation and adhesion of endothelial cells are indispensable for retinal vessel formation (Yang et al., 2015). Our results demonstrate that vascularized area, vessel density and the number of sprouting tips at the vascular front of retinas were significantly increased in PGE₂- or cay10598-treated rat pups compared to the vehicle control group, whereas there was no significant difference in the AH23848-treated retinas. This demonstrates that exaggerated secretion of PGE₂, like

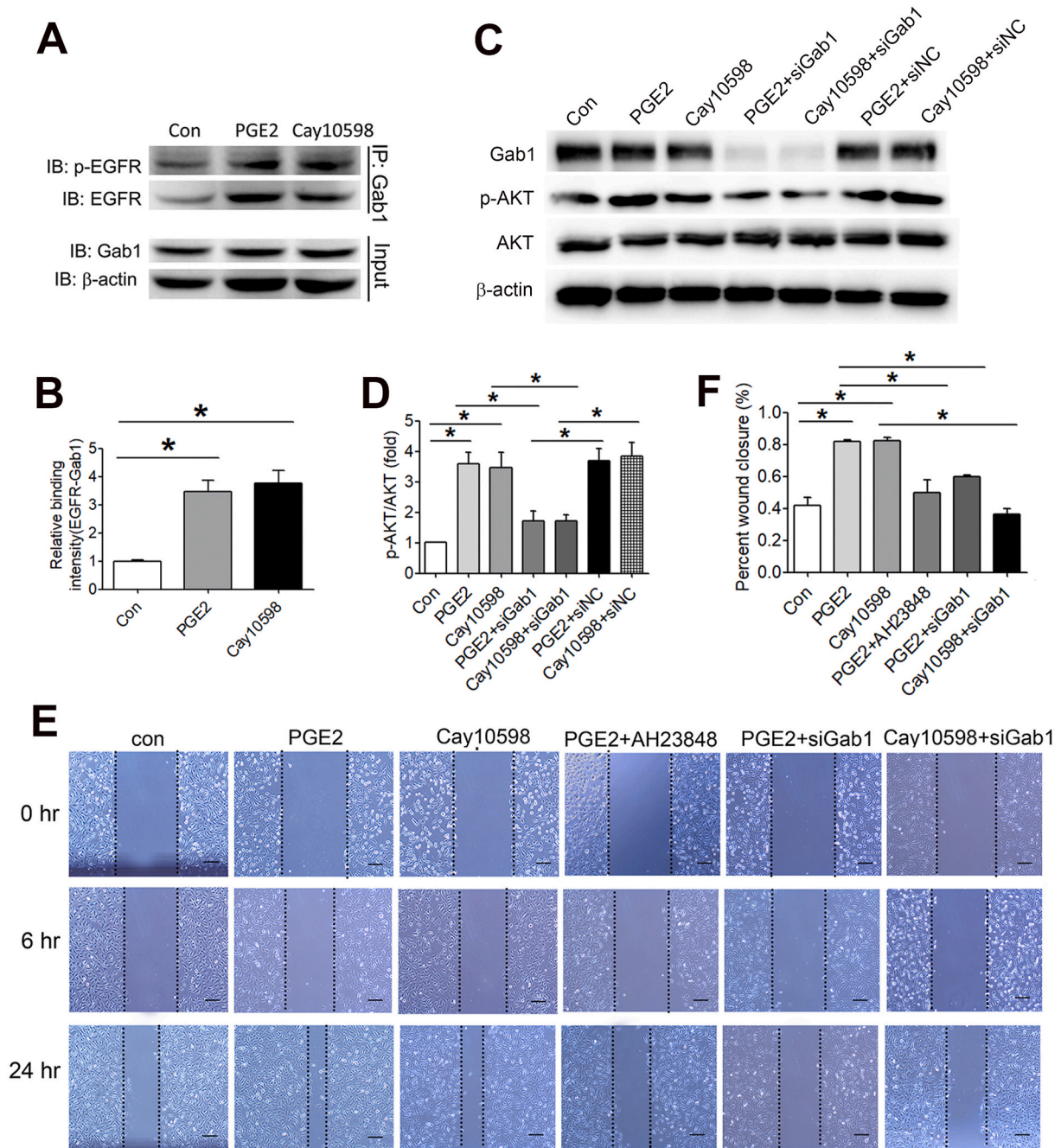


Fig. 7. EGFR recruited Gab1 to mediate the PGE₂-induced Akt activation and cellular proliferation and migration in hRMECs. (A, B) Immunoprecipitation was performed with anti-Gab1 antibody, followed by immunoblotting with p-EGFR and EGFR antibody; N = 5. (C, D) The specific role of Gab1 in Akt phosphorylation of hRMECs. Cells were transiently transfected with the expression vector encoding Gab1 siRNA or the empty vector. Lysates of the cells were immunoblotted with the anti-Gab1 antibody, a phospho-Akt (p-Akt) antibody, an anti-Akt antibody, and an anti- β -actin antibody; N = 5. (E, F) Cell migration was assessed using a wound-healing assay. Images were taken 0, 6 and 24 h after treatment. Migration was estimated by measuring cell numbers within the wounded region. The data are shown as the relative change compared to the control group without treatment. Scale bar, 100 μ m; N = 5. The results are presented as means \pm SEM; **P* < 0.05 for each pair of groups indicated.

that of VEGF-A, PDGF-BB, Erythropoietin and Angiopoietin-2 and metabolic factors like succinate, is involved in the excessive retinal NV during ROP.

It has been reported that PGE₂ receptor EP₄ subtype plays a role in PGE₂-mediated cancer invasiveness by stimulating G alpha protein (G α s) to activate the cAMP/PKA/PAK response element-binding protein signaling pathway (Xia et al., 2014; Parida et al., 2015). However, in our study, blocking the PI3K/Akt pathway or EGFR, but AC or PKA, reversed PGE₂-or cay10598-induced proliferation and migration of hRMECs. This

demonstrates that activated EP₄ is able to phosphorylate and transactivate the EGFR receptor, thus promoting Akt activation required for NF- κ B binding activity and cellular proliferation in hRMECs.

When Gab1 is tyrosine-phosphorylated and recruited by activated EGFR, it goes on to recruit p85 α , the regulatory subunit of PI3K, and to amplify or prolong PI3K activity (Moran et al., 2004; Mouradian et al., 2014). Likewise, we observed that PGE₂ or cay10598 treatment significantly increased the association of EGFR with Gab1 and the phosphorylation of Gab1. Furthermore, siRNA-mediated knockdown of Gab1

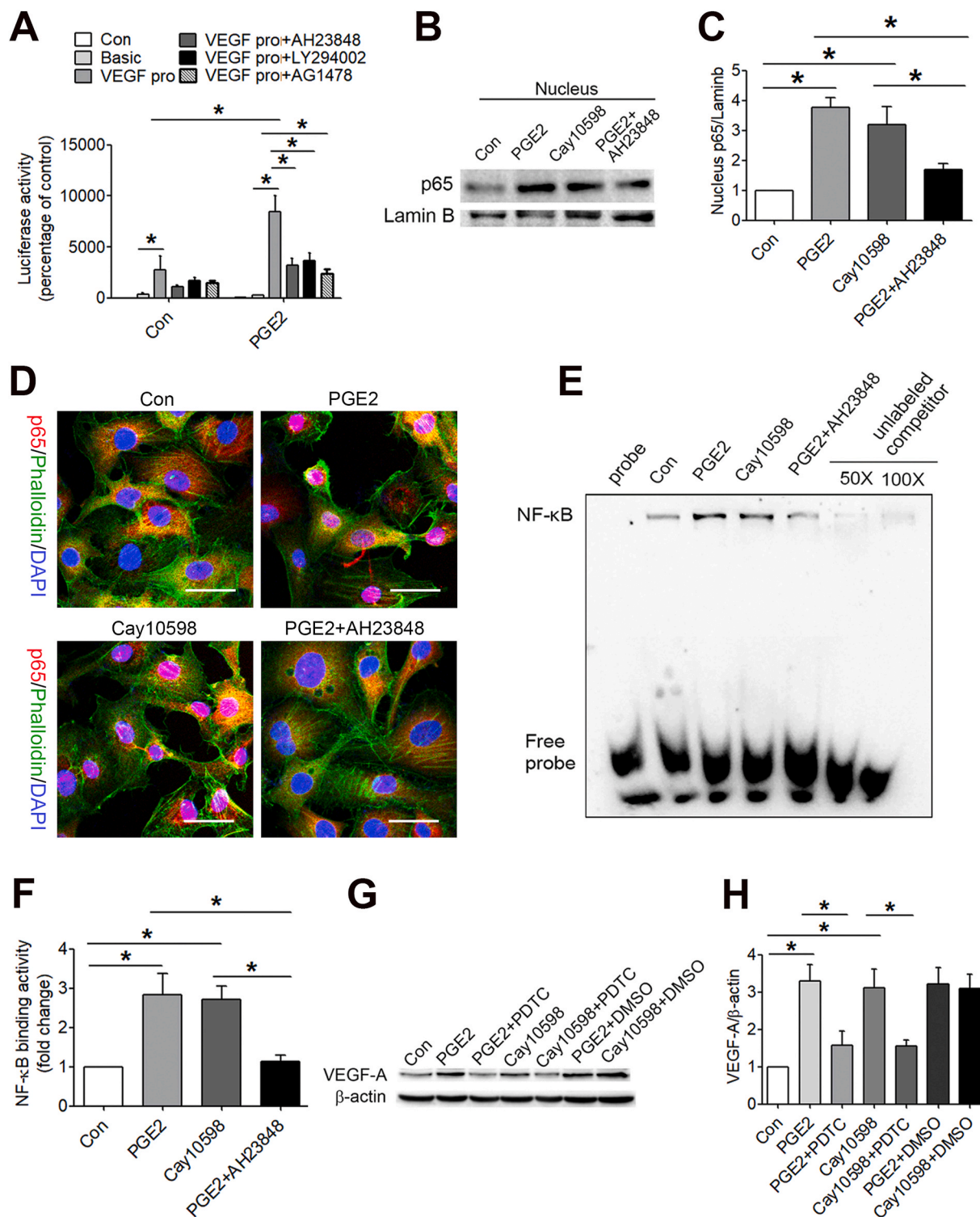


Fig. 8. PGE₂/EP₄R signaling promotes NF-κB binding activity and VEGF-A production in vitro. (A) HEK 293T cells were transfected with VEGF promoter. After 24 h, the relative luciferase activity was measured and normalized by firefly luciferase activity and renilla luciferase activity; N = 5. VEGF pro, VEGF promoter. (B, C) The levels of nuclear p65 were determined Western blot. Lamin B antibody was used to confirm equal nuclear protein loading among samples; N = 5. (D) Immunofluorescence assay evaluation of NF-κB nuclear translocation in hRMECs of each group; scale bar, 25 μm. (E, F) The nuclear proteins were isolated from hRMECs. NF-κB binding activity was determined by EMSA. Representative EMSA results are shown in the left panel (E). The pixel values of the NF-κB binding activity (F); N = 5. (G, H) The levels of VEGF-A in response to different treatments as indicated were determined by western blot. Representative blots are shown, with quantification; N = 5. The results are presented as means ± SEM; *P < 0.05 for each pair of groups indicated.

reversed PGE₂-or cay10598-induced Akt activation and migration of hRMECs. These data suggest that Gab1 is a critical component of PGE₂/EP₄R-mediated EGFR transactivation and Akt activation in proliferation and migration of hRMECs.

To summarize, the present study provides strong evidences that disruption of the PGE₂/EP₄R signaling pathway contributes to the attenuation of the pathogenesis of retinal NV. The underlying mechanism is manifold. Treatment of PGE₂ resulted in transactivation of EGFR and recruitment of Gab1, enhancing cellular proliferation in the ROP model via the Akt signaling pathway. These results indicate that PGE₂/EP₄R mediated hRMECs proliferation by promoting the activation of the EGFR/Gab1/Akt signaling network and that this network may represent a potential therapeutic target for postnatal retinal angiogenesis.

Author contributions

X.W. and Y.Y. designed the experiment, analyzed the data, and wrote the paper. T.X., Z.Z., Y.C., Y.S., Y.L., M.W., Y.W., Q.Y., X.P. performed the experiments and collected and analyzed the data; J.Z., J.C and X.S. designed the experiment and revised the article critically for important intellectual content. All authors gave final approval of the version to be published. X.W. had full access to all the data in this study and takes responsibility for the integrity of the data and the accuracy of the data analysis.

Declaration of competing interest

The authors declare no competing interests.

Funding information

National Natural Science Foundation of China, Grant/Award Numbers: no. 81800845 and 81770941; Jiangsu Key Medical Disciplines, Grant/Award Numbers: ZDXKC2016008; Technology Development Fund, Grant/Award Numbers: CSE12N1701; Wuxi Eminent Medical Talents, Grant/Award Numbers: JCRC005 and QNRC077; Science Foundation of Affiliated Wuxi People's Hospital of Nanjing Medical University, Grant/Award Numbers: RKA201824; Young project of Wuxi health and Family Planning Commission, Grant/Award Numbers: Q201707.

Data availability statement

The datasets generated and analyzed during the current study are available from the corresponding author on reasonable request.

Abbreviations

NV	Neovascularisation
PDR	Proliferative diabetic retinopathy
ROP	Retinopathy of prematurity
PGE ₂	Prostaglandin E ₂
COX	cyclooxygenase
OIR	Oxygen-induced retinopathy
TXA ₂	Thromboxane A ₂
TBXA ₂ R	thromboxane A ₂ receptor
TBXAS1	thromboxane A ₂ synthase
EP ₁₋₄ Rs	E-prostanoid ₁₋₄ receptors
EGFR	EGF receptor
Grb2	Growth factor receptor bound protein 2
Gab1	Grb2-associated binder protein 1
STZ	Streptozotocin
IB4	Isolectin B4
OCT	Optical coherence tomography
H&E	Hematoxylin and eosin
CD105	Endoglin

HRMECs	Human retinal microvascular endothelial cells
INL	Inner nuclear layer
ILM	internal limiting membrane

Appendix A. Supplementary data

Supplementary data to this article can be found online at <https://doi.org/10.1016/j.exer.2021.108507>.

References

- Ansari, K.M., Rundhaug, J.E., Fischer, S.M., 2008. Multiple signaling pathways are responsible for prostaglandin E₂-induced murine keratinocyte proliferation. *Mol. Canc. Res.* 6, 1003–1016.
- Barnett, J.M., Suarez, S., McCollum, G.W., Penn, J.S., 2014. Endoglin promotes angiogenesis in cell- and animal based models of retinal neovascularization. *Invest. Ophthalmol. Vis. Sci.* 55, 6490–6498.
- Bowl, W., Stieger, K., Bokun, M., Schweinfurth, S., Holve, K., Darida, M.A., Lorenz, B., 2016. OCT-based macular structure-function correlation in dependence on birth weight and gestational age-the giessen long-term ROP study. *Invest. Ophthalmol. Vis. Sci.* 57, T235–T241.
- Buchanan, F.G., Gorden, D.L., Matta, P., Shi, Q., Matrisian, L.M., DuBois, R.N., 2006. Role of beta-arrestin 1 in the metastatic progression of colorectal cancer. *Proc. Natl. Acad. Sci. U.S.A.* 103, 1492–1497.
- Buchanan, F.G., Wang, D., Bargiacchi, F., DuBois, R.N., 2003. Prostaglandin E₂ regulates cell migration via the intracellular activation of the epidermal growth factor receptor. *J. Biol. Chem.* 278, 35451–35457.
- Capra, V., Back, M., Angiolillo, D.J., Cattaneo, M., Sakariassen, K.S., 2014. Impact of vascular thromboxane prostanoid receptor activation on hemostasis, thrombosis, oxidative stress, and inflammation. *J. Thromb. Haemostasis* 12, 126–137.
- Castro, M.R., Lutz, D., Edelman, J.L., 2004. Effect of COX inhibitors on VEGF-induced retinal vascular leakage and experimental corneal and choroidal neovascularization. *Exp. Eye Res.* 79, 275–285.
- Cernichiaro-Espinosa, L.A., Olguin-Manriquez, F.J., Henaine-Berra, A., Garcia-Aguirre, G., Quiroz-Mercado, H., Martinez-Castellanos, M.A., 2016. New insights in diagnosis and treatment for Retinopathy of Prematurity. *Int. Ophthalmol.* 36, 751–760.
- Chen, X., Mangalesh, S., Dandridge, A., Tran-Viet, D., Wallace, D.K., Freedman, S.F., Toth, C.A., 2018. Spectral-domain OCT findings of retinal vascular-avascular junction in infants with retinopathy of prematurity. *Ophthalmol. Retina* 2, 963–971.
- Cheng, T., Cao, W., Wen, R., Steinberg, R.H., LaVail, M.M., 1998. Prostaglandin E₂ induces vascular endothelial growth factor and basic fibroblast growth factor mRNA expression in cultured rat Muller cells. *Invest. Ophthalmol. Vis. Sci.* 39, 581–591.
- Chung, A.S., Ferrara, N., 2011. Developmental and pathological angiogenesis. *Annu. Rev. Cell Dev. Biol.* 27, 563–584.
- Dallas, N.A., Samuel, S., Xia, L., Fan, F., Gray, M.J., Lim, S.J., Ellis, L.M., 2008. Endoglin (CD105) a marker of tumor vasculature and potential target for therapy. *Clin. Canc. Res.* 14, 1931–1937.
- Deliyanti, D., Miller, A.G., Tan, G., Binger, K.J., Samson, A.L., Wilkinson-Berka, J.L., 2012. Neovascularization is attenuated with aldosterone synthase inhibition in rats with retinopathy. *Hypertension* 59, 607–613.
- Erol, M.K., Ozdemir, O., Coban, D.T., Bilgin, A.B., Dogan, B., Sari, E.S., Toslak, D., 2014. Macular findings obtained by spectral domain optical coherence tomography in retinopathy of prematurity. *J. Ophthalmol.* 2014, 468653.
- Feenstra, D.J., Seleci, M., Denk, N., Fauser, S., Drawnel, F.M., Jayagopal, A., 2019. Indocyanine green molecular angiography of choroidal neovascularization. *Exp. Eye Res.* 180, 122–128.
- Fong, D.S., Aiello, L.P., Ferris, F.R., Klein, R., 2004. Diabetic retinopathy. *Diabetes Care* 27, 2540–2553.
- Han, N., Xu, H., Yu, N., Wu, Y., Yu, L., 2020. MiR-203a-3p inhibits retinal angiogenesis and alleviates proliferative diabetic retinopathy in oxygen-induced retinopathy (OIR) rat model via targeting VEGFA and HIF-1alpha. *Clin. Exp. Pharmacol. Physiol.* 47, 85–94.
- Han, X., Kong, J., Hartnett, M.E., Wang, H., 2019. Enhancing retinal endothelial glycolysis by inhibiting UCP2 promotes physiologic retinal vascular development in a model of retinopathy of prematurity. *Invest. Ophthalmol. Vis. Sci.* 60, 1604–1613.
- Hartnett, M.E., 2020. Retinopathy of prematurity: evolving treatment with anti-vascular endothelial growth factor. *Am. J. Ophthalmol.* 218, 208–213.
- Hata, A.N., Breyer, R.M., 2004. Pharmacology and signaling of prostaglandin receptors: multiple roles in inflammation and immune modulation. *Pharmacol. Ther.* 103, 147–166.
- Laatikainen, L., Ojamo, M., Rudanko, S.L., Summanen, P., Kiukaanniemi, S.K., Tuomilehto, J., Herrala, S., Uusitalo, H., 2016. Improving visual prognosis of the diabetic patients during the past 30 years based on the data of the Finnish Register of Visual Impairment. *Acta Ophthalmol.* 94, 226–231.
- Laouri, M., Chen, E., Looman, M., Gallagher, M., 2011. The burden of disease of retinal vein occlusion: review of the literature. *Eye (Lond)* 25, 981–988.
- Lee, A.C., Lee, A.C., Maldonado, R.S., Sarin, N., O'Connell, R.V., Wallace, D.K., Freedman, S.F., Cotten, M., Toth, C.A., 2011. Macular features from spectral-domain optical coherence tomography as an adjunct to indirect ophthalmoscopy in retinopathy of prematurity. *Retina* 31, 1470–1482.
- Lucotti, S., Cerutti, C., Soyer, M., Bernabé, A.M.J., Gomes, A.L., Allen, P.D., Smart, S., Markelc, B., Watson, K., Armstrong, P.C., Mitchell, J.A., Warner, T.D., Ridley, A.J.,

- Muschel, R.J., 2019. Aspirin blocks formation of metastatic intravascular niches by inhibiting platelet-derived COX-1/thromboxane A2. *J. Clin. Invest.* 129, 1845–1862.
- Moran, A.E., Hunt, D.H., Javid, S.H., Redston, M., Carothers, A.M., Bertagnoli, M.M., 2004. Apc deficiency is associated with increased Egfr activity in the intestinal enterocytes and adenomas of C57BL/6J-Min/+ mice. *J. Biol. Chem.* 279, 43261–43272.
- Mouradian, M., Kikawa, K.D., Johnson, E.D., Beck, K.L., Pardini, R.S., 2014. Key roles for GRB2-associated-binding protein 1, phosphatidylinositol-3-kinase, cyclooxygenase 2, prostaglandin E2 and transforming growth factor alpha in linoleic acid-induced upregulation of lung and breast cancer cell growth. *Prostaglandins Leukot. Essent. Fatty Acids* 90, 105–115.
- Mynampati, B.K., Sambhav, K., Grover, S., Chalam, K.V., 2017. Inhibition of proliferation of retinal vascular endothelial cells more effectively than choroidal vascular endothelial cell proliferation by bevacizumab. *Int. J. Ophthalmol.* 10, 15–22.
- Naderi, A., Zahed, R., Aghajanzpour, L., Amoli, F.A., Lashay, A., 2019. Long term features of diabetic retinopathy in streptozotocin-induced diabetic Wistar rats. *Exp. Eye Res.* 184, 213–220.
- Nandgaonkar, B.N., Rotschild, T., Yu, K., Higgins, R.D., 1999. Indomethacin improves oxygen-induced retinopathy in the mouse. *Pediatr. Res.* 46, 184–188.
- Olivares, A.M., Althoff, K., Chen, G.F., Wu, S., Morrisson, M.A., DeAngelis, M.M., Haider, N., 2017. Animal models of diabetic retinopathy. *Curr. Diabetes Rep.* 17, 93.
- Parida, S., Parekh, A., Dey, G., Ghosh, S.C., Mandal, M., 2015. Molecular inhibition of prostaglandin E2 with GW627368X: therapeutic potential and preclinical safety assessment in mouse sarcoma model. *Canc. Biol. Ther.* 16, 922–932.
- Reynolds, J.D., 2014. Insights in ROP. *Am. Orthopt. J.* 64, 43–53.
- Rivera, J.C., Noueihed, B., Omri, S., Barrueco, J., Hilberg, F., Chemtob, S., 2015. BIBF1120 (vargatef) inhibits preretinal neovascularization and enhances normal vascularization in a model of vasoproliferative retinopathy. *Invest. Ophthalmol. Vis. Sci.* 56, 7897–7907.
- Rothman, A.L., Tran-Viet, D., Gustafson, K.E., Goldstein, R.F., Maguire, M.G., Tai, V., Sarin, N., Tong, A.Y., Huang, J.Y., Kupper, L., Cotten, C.M., Freedman, S.F., Toth, C.A., 2015. Poorer neurodevelopmental outcomes associated with cystoid macular edema identified in preterm infants in the intensive care nursery. *Ophthalmology* 122, 610–619.
- Sapieha, P., Joyal, J.S., Rivera, J.C., Duchemin, E.K., Sennlaub, F., Hardy, P., Lachapelle, P., Chemtob, S., 2010. Retinopathy of prematurity: understanding ischemic retinal vasculopathies at an extreme of life. *J. Clin. Invest.* 120, 3022–3032.
- Schoenberger, S.D., Kim, S.J., Sheng, J.S., Rezaei, K.A., Lalezary, M., Cherney, E., 2012. Increased prostaglandin E2 (PGE2) levels in proliferative diabetic retinopathy, and correlation with VEGF and inflammatory cytokines. *Invest. Ophthalmol. Vis. Sci.* 53, 5906–5911.
- Sennlaub, F., Valamanesh, F., Vazquez-Tello, A., Asrar, A.M.E., Checchin, D., Brault, S., Gobeil, F., Beauchamp, M.H., Mwaikambo, B., Courtois, Y., Geboes, K., Varma, D.R., Lachapelle, P., Ong, H., Behar-Cohen, F., Chemtob, S., 2003. Cyclooxygenase-2 in human and experimental ischemic proliferative retinopathy. *Circulation* 108, 198–204.
- Shan, K., Liu, C., Liu, B.H., Chen, X., Dong, R., Liu, X., Zhang, Y.Y., Liu, B., Zhang, S.J., Wang, J.J., Zhang, S.H., Wu, J.H., Zhao, C., Yan, B., 2017. Circular noncoding RNA HIPK3 mediates retinal vascular dysfunction in diabetes mellitus. *Circulation* 136, 1629–1642.
- Stahl, A., Connor, K.M., Sapieha, P., Chen, J., Dennison, R.J., Krah, N.M., Seaward, M.R., Willett, K.L., Aderman, C.M., Guerin, K.I., Hua, J., Löfqvist, C., Hellström, A., Smith, L.E.H., 2010. The mouse retina as an angiogenesis model. *Invest. Ophthalmol. Vis. Sci.* 51, 2813–2826.
- Stoica, F., Emami, A.C., Andreescu, N., Stanciu, A., Zimbru, C.G., Puiu, M., 2018. Clinical relevance of retinal structure in children with laser-treated retinopathy of prematurity versus controls - using optical coherence tomography. *Acta Ophthalmol.* 96, e222–e228.
- Tan, S., Chen, X.L., Xu, M.Y., Huang, X.L., Liu, H.L., Jiang, J., Lu, Y., Peng, X.J., Wu, B., 2017. PGE2/EP4 receptor attenuated mucosal injury via beta-arrestin1/Src/EGFR-mediated proliferation in portal hypertensive gastropathy. *Br. J. Pharmacol.* 174, 848–866.
- Tzeng, T.F., Hong, T.Y., Tzeng, Y.C., Liou, S.S., Liu, I.M., 2015. Consumption of polyphenol-Rich Zingiber Zerumbet Rhizome extracts protects against the breakdown of the blood-retinal barrier and retinal inflammation induced by diabetes. *Nutrients* 7, 7821–7841.
- Wang, B., Li, P.K., Ma, J.X., Chen, D., 2018. Therapeutic effects of a novel phenylphthalimide analog for corneal neovascularization and retinal vascular leakage. *Invest. Ophthalmol. Vis. Sci.* 59, 3630–3642.
- Wang, W.Z., Chen, J.L., Mao, J.Y., Li, H.L., Wang, M.F., Zhang, H., Li, H.T., Chen, W., 2018. Genistein ameliorates non-alcoholic fatty liver disease by targeting the thromboxane A2 pathway. *J. Agric. Food Chem.* 66, 5853–5859.
- Wang, X.L., Gao, Y., Song, J., Tang, C., Wang, M., Que, L.L., Liu, L., Zhu, G.Q., Chen, Q., Yao, Y., Xu, Y., Li, J.T., Li, Y.H., 2017. The TIR/BB-loop mimetic AS-1 prevents non-alcoholic steatohepatitis and hepatic insulin resistance by inhibiting NLRP3-ASC inflammasome activation. *Br. J. Pharmacol.* 174, 1841–1856.
- Wilkinson-Berka, J.L., Alousis, N.S., Kelly, D.J., Gilbert, R.E., 2003. COX-2 inhibition and retinal angiogenesis in a mouse model of retinopathy of prematurity. *Invest. Ophthalmol. Vis. Sci.* 44, 974–979.
- Wilkinson-Berka, J.L., Tan, G., Jaworski, K., Harbig, J., Miller, A.G., 2009. Identification of a retinal aldosterone system and the protective effects of mineralocorticoid receptor antagonism on retinal vascular pathology. *Circ. Res.* 104, 124–133.
- Wu, Q., Wang, H., Zhao, X., Shi, Y., Jin, M., Wan, B., Xu, H., Cheng, Y., Ge, H., Zhang, Y., 2013. Identification of G-protein-coupled receptor 120 as a tumor-promoting receptor that induces angiogenesis and migration in human colorectal carcinoma. *Oncogene* 32, 5541–5550.
- Wu, T., 2005. Cyclooxygenase-2 and prostaglandin signaling in cholangiocarcinoma. *Biochim. Biophys. Acta* 1755, 135–150.
- Wu, W., Hu, Y.P., Li, J.T., Zhu, W.N., Ha, T.Z., Que, L.L., Liu, L., Zhu, Q., Chen, Q., Chen, Q., Xu, Y., Li, C.F., Li, Y.H., 2014. Silencing of Pellino1 improves post-infarct cardiac dysfunction and attenuates left ventricular remodeling in mice. *Cardiovasc. Res.* 102, 46–55.
- Xia, S., Ma, J., Bai, X.M., Zhang, H., Cheng, S.Y., Zhang, M., Zhang, L., Du, M.Z., Wang, Y.P., Li, H., Rong, R., Shi, F., Yang, Q.Y., Leng, J., 2014. Prostaglandin E2 promotes the cell growth and invasive ability of hepatocellular carcinoma cells by upregulating c-Myc expression via EP4 receptor and the PKA signaling pathway. *Oncol. Rep.* 32, 1521–1530.
- Yang, W.J., Hu, J.H., Uemura, A., Tetzlaff, F., Augustin, H.G., Fischer, A., 2015. Semaphorin-3C signals through Neuropilin-1 and PlexinD1 receptors to inhibit pathological angiogenesis. *EMBO Mol. Med.* 7, 1267–1284.
- Yanni, S.E., Barnett, J.M., Clark, M.L., Penn, J.S., 2009. The role of PGE2 receptor EP4 in pathologic ocular angiogenesis. *Invest. Ophthalmol. Vis. Sci.* 50, 5479–5486.
- Zepeda, E.M., Shariff, A., Gillette, T.B., Grant, L., Ding, L., Hornoch, K.T., Cabrera, M.T., 2018. Vitreous bands identified by handheld spectral-domain optical coherence tomography among premature infants. *Jama Ophthalmol.* 136, 753–758.
- Zhang, B.F., Jiang, H., Chen, J., Hu, Q., Yang, S., Liu, X.P., Liu, G., 2020. LncRNA H19 ameliorates myocardial infarction-induced myocardial injury and maladaptive cardiac remodeling by regulating KDM3A. *J. Cell Mol. Med.* 24, 1099–1115.